Journal of Energy Chemistry xxx (xxxx) xxx

Contents lists available at ScienceDirect

Journal of Energy Chemistry

journal homepage: www.elsevier.com/locate/jechem

http://www.journals.elsevier.com/journal-of-energy-chemistry/

N-heterocyclic carbene as a promising metal-free electrocatalyst with high-efficiency for nitrogen reduction to ammonia

Q1 Hongyan Li[a], Le Yang[b], Zhongxu Wang[a], Peng Jin[b,*], Jingxiang Zhao[a,*], Zhongfang Chen[c,*]

[a] College of Chemistry and Chemical Engineering, and Key Laboratory of Photonic and Electronic Bandgap Materials, Ministry of Education, Harbin Normal University, Harbin 150025, Heilongjiang, China
[b] School of Materials Science and Engineering, Hebei University of Technology, Tianjin 300130, China
[c] Department of Chemistry, University of Puerto Rico, Rio Piedras Campus, San Juan, PR 00931, USA

ARTICLE INFO

Article history:
Received 17 September 2019
Revised 21 October 2019
Accepted 23 October 2019
Available online xxx

Keywords:
Nitrogen reduction reaction
N-heterocyclic carbenes
Overpotential
Density functional theory

ABSTRACT

Electrocatalytic nitrogen reduction reaction (NRR) at ambient conditions holds great promise for sustainably synthesizing ammonia (NH_3), while developing highly-efficient, long-term stable, and inexpensive catalysts to activate the inert N≡N bond is a key scientific issue. In this work, on the basis of the concept "N-heterocyclic carbenes (NHCs)", we propose a carbon decorated graphitic-carbon nitride (C/g-C_3N_4) as novel metal-free NRR electrocatalyst by means of density functional theory (DFT) computations. Our results reveal that the introduced C atom in g-C_3N_4 surface can be regarded as NHCs and catalytic sites for activating N≡N bond, and are stabilized by the g-C_3N_4 substrate due to sterically disfavored dimerization. Especially, this NHCs-based heterogeneous catalysis can efficiently reduce the activated N_2 molecule to NH_3 with a low overpotential of 0.05 V via an enzymatic mechanism. Our work is the first report of NHCs-based electrocatalyst for N_2 fixation, thus opening an alternative avenue for advancing sustainable NH_3 production.

1. Introduction

The ammonia (NH_3) synthesis from molecular nitrogen (N_2) was regarded as one of the greatest inventions in 20th century because NH_3 is an essential building block for manufacturing synthetic chemicals, such as fertilizers, medicaments, dyes, explosives, and resins [1,2], thus spawning three Nobel Prizes in Chemistry (1918, 1931, 2007). In addition, NH_3 is also a promising green energy carrier and potential transport fuel to advance a low-carbon society due to its large hydrogen capacity (17.6 wt%) and high energy density (4.3 kWh h^{-1}) [3,4]. Thus, the ever-increasing demand for NH_3 has stimulated great interest in artificial N_2-to-NH_3 conversion. Currently, industrial N_2 fixation for NH_3 production still relies on the traditional Haber-Bosch process [5], which requires both high temperature (~500 °C) and high pressure (200–300 atm) [6]. Also, this process needs to consume large quantities of H_2. It accounts for ~1% of the world's annual energy consumption and produces about 300 t of greenhouse gases (CO_2) [7]. Therefore, it is highly desirable to develop alternative strategy for NH_3 production to replace the energy-intensive Harber–Bosch process.

Motivated by the biological N_2 fixation, in which the nitrogenase enzymes catalyze NH_3 synthesis with the existence of H_2O, electrons, and atmospheric N_2 under mild conditions [8], photocatalytic or electrocatalytic N_2 reduction reaction (NRR) has been regarded as being quite promising for sustainable NH_3 production because the raw ingredients (water and air) and driving force (renewable solar and wind energy) are environmentally friendly, inexpensive, and readily accessible [9–11]. However, the extremely high stability of N_2 requires stable, efficient, and inexpensive catalysts to lower the energy consumption, enhance the rate, and increase the selectivity [12–24]. Thus, searching for novel catalysts for NRR by experimental and theoretical methods has been a key scientific issue in recent years [9–11].

Currently, metal-based materials, including transition metals with flat and step surfaces especially noble metals, such as platinum, palladium, metal nitrides, and metal oxides, are generally employed in the NRR [15–18]. However, several disadvantages, including low selectivity, poor durability, high-cost, and limited availability seriously hinder their large-scale applications. Compared to metal-based catalysts, metal-free carbon materials are emerging as one of most promising alternatives due to their overwhelming inherent characteristics, such as excellent stability, abundant natural resources, high surface area, controllable structures, resistance to acids and bases, and environmental friendliness [19–22]. Thus,

Q2 * Corresponding authors.
E-mail addresses: china.peng.jin@gmail.com (P. Jin), zhaojingxiang@hrbnu.edu.cn (J. Zhao), zhongfangchen@gmail.com (Z. Chen).

https://doi.org/10.1016/j.jechem.2019.10.016
2095-4956/

the carbon nanomaterials have been widely utilized in many electrochemical reactions, such as oxygen reduction/evolution, carbon dioxide reduction, hydrogen evolution reactions [23–28].

In the recent years, N-heterocyclic carbenes (NHCs) have evoked great interest due to their structural diversity, high reactivity, and multiple applications as catalysts for some of the most important catalytic transformations in the chemical industry [29]. In particular, the filled σ-frontier and vacant π-frontier orbitals in NHCs endow them with high reactivity to activate small molecules, such as H_2 and CO [30–33]. Although NHCs have opened up new areas of research as the most powerful tools in organic chemistry, steric hindrance via bulky substituents adjacent to the carbene carbon is generally employed to prevent their dimerization to the corresponding olefin [31]. In addition, introducing the NHCs concept to the heterogeneous systems was shown to be an alternative strategy to stabilize NHCs [34,35]. Especially, the combination of NHCs (*high reactivity*) and the solid catalyst (*ease of separation, purification and recyclability*) will make the heterogeneous system have wider applications for the synthesis of fine chemicals on an industrial scale [35]. Therefore, choosing a suitable support to stabilize NHCs is highly desirable for their industrial applications.

As an excellent substrate, graphitic carbon nitride (g-C_3N_4) offers a number of inherent advantages, such as possessing long-term stability, maintaining the metal atoms in their neutral state, and directly providing the hydrogen source [36]. Thus, g-C_3N_4 has been widely utilized to support noble-metal catalysts for various chemical reactions [37,38]. In terms of the high reactivity of NHCs and the great potential of g-C_3N_4 as substrate, an interesting question naturally arises: can one combine the respective advantages of NHCs and g-C_3N_4 to design a new class of heterogeneous electrocatalyst for the NRR?

To answer this question, in this work, by means of extensive density functional theory (DFT) computations, we incorporated one C atom into g-C_3N_4 surface (C/g-C_3N_4) to explore its potential as heterogeneous NHCs-based NRR catalysts for NH_3 production. Our results revealed that C/g-C_3N_4 exhibits NHCs nature due to its sp^2-hybridized lone pair and unoccupied *p*-orbital, which are responsible for its extremely high NRR catalytic activity with a low overpotential of 0.05 V via an enzymatic pathway. Thus, the decoration of g-C_3N_4 sheet with a single C atom is very promising way to obtain highly-efficient NRR electrocatalyst for NH_3 production.

2. Computational details

All the spin-polarized density functional theory (DFT) computations were performed by using the Dmol^3 code [39,40]. The Perdew–Burke–Ernzerhof (PBE) functional of the generalized gradient approximation (GGA) was used to describe the exchange correlation function [41]. The van der Waals interactions were determined using the empirical correction in Grimme's scheme (i.e., DFT+D2) [42], and the double numerical plus polarization (DNP) basis set was used for all elements, since its accuracy was revealed to be comparable to that of Pople's 6–31G** basis set. Self-consistent field computations were performed with a convergence criterion of 10^{-6} a.u. on the total energy and electronic computations. To ensure high quality results, the real-space global orbital cutoff radius was chosen as high as 5.2 Å in all the computations.

A $2\times2\times1$ supercell of g-C_3N_4 was built that consists of 24 C and 32 N atoms with a vacuum space of 20 Å to avoid the interactions between two periodic images. The Brillouin zone was sampled with a Monkhorst–Pack mesh with a $5\times5\times1$ grid in reciprocal space during geometry optimizations. The Hirshfeld charge analysis was employed to compute the charge transfer [43]. Molecular dynamics (MD) simulations were adopted to evaluate the thermodynamic stability of C/g-C_3N_4 for 10.0 ps with a time step of 1.0 fs under 500 K using the Nose-Hoover method.

The computational hydrogen electrode (CHE) technique was adopted simulate the electrochemical reactions [44,45]. In this technique, the change in Gibbs free energy (ΔG) for each elementary step was determined by: $\Delta G=\Delta E+\Delta E_{ZPE}-T\Delta S+\Delta G_{pH}+\Delta G_U$, where ΔE is the reaction energy that can be directly obtained by analyzing the DFT total energies. ΔE_{ZPE} and ΔS were the difference of zero point energy and entropy between the products and the reactants at room temperature ($T=298.15$ K), respectively, which can be computed from the vibrational frequencies. Notably, only the vibrational modes of the adsorbed intermediates were explicitly computed, while the catalyst surface was fixed by assuming that the vibrations of the solid catalysts can be negligible. The entropies of the free molecules were taken from the NIST database, while the entropy contribution from the adsorbed state was neglected. ΔG_{pH} is the free energy correction of pH, which can be calculated by $\Delta G_{pH}=k_BT\times pH\times \ln10$, and the pH value was set to be zero in this work. ΔG_U is the free energy contributions related to the applied electrode potential (U), i.e., $\Delta G_U=-neU$, where n is the number of electrons transferred. Note that the stabilization effects of water on the NRR is smaller than 0.10 eV per hydrogen bond [46,47], previous theoretical studies have demonstrated that NH_2* species is slightly more stable in the presence of water, while N* species will not be affected by the bulk water layer [48]. Thus, considering the significant increase of the computational cost, explicit solvent model for water was not used in this work. To obtain the proton-electron transfer energy barriers of each elementary steps, the transition states were located by using the synchronous method with conjugated gradient refinements, which involves linear synchronous transit (LST) maximization, followed by repeated conjugated gradient (CG) minimizations, and then quadratic synchronous transit (QST) maximizations and repeated CG minimizations until a transition state was located [49].

3. Results and discussion

3.1. Structures, properties, and stabilities of C/g-C_3N_4

The optimized lattice parameter of the g-C_3N_4 nanosheet in this study is 7.15 Å, and the lengths of the C–N bonds range from 1.33 to 1.47 Å, which are in good accordance with previous theoretical reports [37]. To find the most favorable deposition sites for single C atom, various sites on the g-C_3N_4 supercell were considered as shown in Fig. S1 in Supporting Information. After fully structural optimization, our results demonstrated that the single C atom is preferably adsorbed at the corner of the sixfold cavity (Fig. 1a), and the binding energy (E_{bind}) is computed to be −4.46 eV. Here, the E_{bind} value was determined as: $E_{bind}=E_{C/C3N4}-E_{C3N4}-E_C$, where $E_{C/C3N4}$, E_{C3N4}, and E_C represent the total energies of doped and pristine g-C_3N_4 sheets as well as an isolated C atom, respectively. Remarkably, we also considered the binding of single C atom on other sites of C_3N_4, including the hexagonal hole site and 2-fold-coordinated N atoms. After full relaxation, however, these two configurations spontaneously converted to the most stable one (Fig. 1a), indicative of its high thermodynamic stability, which provides significant advantages for experimental synthesis of the designed C/g-C_3N_4 catalyst. On the other hand, we performed molecular dynamics simulations to examine the thermal stability of C/g-C_3N_4 at 500 K. No notable geometry distortion for C/C_3N_4 was observed after 10 ps simulations (Fig. S2), suggesting its high thermal stability.

Interestingly, various doped g-C_3N_4 with nonmetal elements, including P, B, C, O, and S, have been experimentally synthesized in recent years, and they exhibit very good catalytic performance for many important chemical reactions [50]. Our interest is in C-doping into C_3N_4, since we mainly studied the potential of

Please cite this article as: H. Li, L. Yang and Z. Wang et al., N-heterocyclic carbene as a promising metal-free electrocatalyst with high-efficiency for nitrogen reduction to ammonia, Journal of Energy Chemistry, https://doi.org/10.1016/j.jechem.2019.10.016

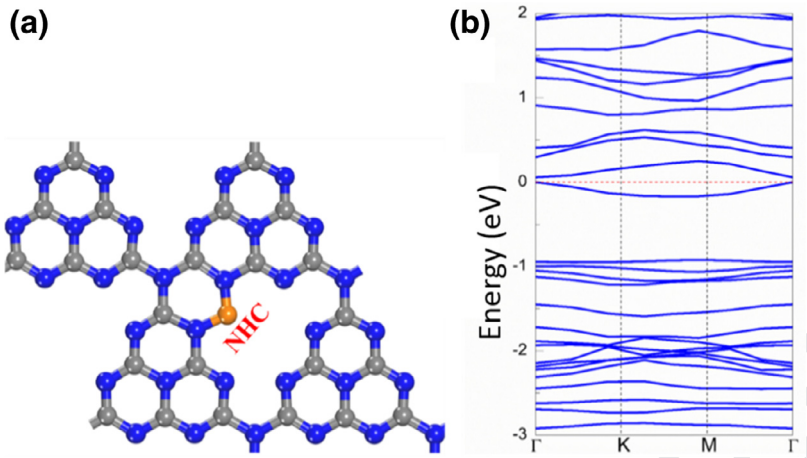

Fig. 1. (a) The most stable configuration and (b) band structure of single C atom adsorbed on g-C_3N_4. The Fermi level was set to zero.

NHC-based heterogeneous catalyst for the NRR, which could derive from doped C_3N_4 with C atom, not other non-carbon dopants, such as B, P, and S. Remarkably, some facile techniques have been proposed to synthesize C self-doped C_3N_4 by controlling the synthetic conditions, such as carbon source, preparation process [51–53]. For example, Wang et al. synthesized carbon quantum dots (CQDs) implanted in the surface plane of g-C_3N_4 by thermal polymerization of freeze-dried urea and CQDs precursor [51]. Gao et al. prepared ultrathin carbon rich nanosheets via an extremely facile hexamethylenetetramine activation approach at bulk scale [52], while Bao et al. successfully synthesized C-doped g-C_3N_4 using anionic polyacrylamide as the intercalator and carbon source via the thermal treatment method [53]. Overall, the high stability of C/g-C_3N_4 and the exciting experimental advances on fabricating C-doped g-C_3N_4 endow the great promise for the experimental realization of C/g-C_3N_4 and its applications as catalysts.

In general, excellent electrical conductivity of a catalyst could ensure good charge transfer for efficient electrochemical reactions. Thus, the band structures of the g-C_3N_4 before and after C decoration were computed to estimate the electrical conductivity (Figs. S3 and 1b). Our results showed that the pristine g-C_3N_4 is a semiconductor with the band gap of 1.21 eV, which is well consistent with previous theoretical studies [54]. After the incorporation of C atom, however, the band gap of g-C_3N_4 is greatly decreased to about 0.06 eV (Fig. 1b) due to the introduction of impurity states, and the computed band gap is, suggesting good electronic conductivity of C/g-C_3N_4, which could promote the electron transfer in the electrocatalytic reactions.

Another important issue is to examine whether the C/g-C_3N_4 coincides in the characteristics of NHCs. Structurally, the proposed C/g-C_3N_4 is a heterocyclic material, and contains a two-coordinated C atom within a 6-membered ring. Meanwhile, two N atoms of g-C_3N_4 adjacent to the C-dopant could help to stabilize the species. The length of the two newly formed C–N bond is 1.37 Å, which is the same as that of the well-established NHCs, e.g., 1, 3-di (adamantyl)−2-ylidene. Furthermore, C/g-C_3N_4 exhibits a singlet ground-state electronic configuration, which is 0.11 eV lower in energy than the triplet state.

We further carried out natural bond orbital (NBO) analysis for a large cluster model using the Gaussian 03 software [55] at the PBE−D/6 − 31G* level of theory (Fig. 2a). The NBO results revealed that only C1 has a lone pair (LP) among all the carbon atoms, corresponding to the highest occupied molecular orbital (HOMO) (Fig. 2b). The two adjacent N atoms stabilize C1 via both the σ-electron-withdrawing and π-electron-donating effects, as suggested by the polarity of the C1-N σ-bonds (68.78% at each N) and large E (2) energy (65.24 kcal mol^{-1}) in the second-order perturbative analysis for the donor-acceptor interaction between each N-LP and C1-2p_z orbital. The occupation of the originally empty C1-2p_z orbital is thus substantial (0.75 e). As a result, C1 has a slightly positive natural population analysis (NPA) charge close to zero (+0.114), which is much smaller than all the other carbon atoms with three N neighbors in the model (>+0.5). All these features resemble those of a typical N-heterocyclic carbene. With both electron-abundant LP and partially occupied p_z orbital, C1 could serve as a unique active center in catalysis, which can be also revealed by using the periodic model as shown in Fig. S4.

3.2. N_2 adsorption on C/g-C_3N_4

After confirming that C/g-C_3N_4 possesses NHC's nature, we explored its chemical activity towards N_2 adsorption, which is the first and crucial step for the NRR, since it determinates the following reaction pathway. To obtain the stable configuration for N_2 adsorption, two adsorption patterns, including end- and side-on adsorption, were considered for N_2 molecule on different nonequivalent positions of the C/g-C_3N_4 sheet.

For pristine g-C_3N_4 monolayer, the physical adsorption of N_2 (E_{ads} = −0.13 eV) suggest very low activity of N_2 on g-C_3N_4 (Fig. S5). While for the case of C/g-C_3N_4, due to the well-known high reactivity of the NHCs, the NHC is the energetically favorable adsorption site for the N_2 molecule, and both end- and side-on adsorption configurations are stable (Fig. 3) with the adsorption energies of −1.42 and −0.75 eV, respectively. The corresponding free energy changes are −0.71 and −0.05 eV after considering the corrections of zero-point energy and entropy, thus suggesting a strong chemisorption. Consistently, chemical bonds are formed between the adsorbed N_2 molecule and C/g-C_3N_4 according to the short distances of 1.31 and 1.44 Å between them. The strong chemisorption elongates the N–N bond length from 1.10 Å in free N_2 to 1.16 Å for adsorbed one in end-on manner with the formation of one C–N bond, which is slightly shorter than that of in side-on one (1.27 Å) with the formation of two C–N bonds. The elongation of the N–N bond in the adsorbed N_2 molecule could originate from the charge transfer from the C/g-C_3N_4 to the adsorbed N_2 molecule, which occupy the empty 2π^* orbitals of N_2. Less charge transfer occurs in the end-on adsorption compared with the side-on counterpart (0.05e vs. 0.10 e), resulting in the shorter N–N bond length (1.16 Å) in the end-on manner (1.27 Å for the side-on adsorption). Overall, the N_2 molecule can be activated to different degrees after adsorption on this C/g-C_3N_4, especially in the side-on configuration.

Please cite this article as: H. Li, L. Yang and Z. Wang et al., N-heterocyclic carbene as a promising metal-free electrocatalyst with high-efficiency for nitrogen reduction to ammonia, Journal of Energy Chemistry, https://doi.org/10.1016/j.jechem.2019.10.016

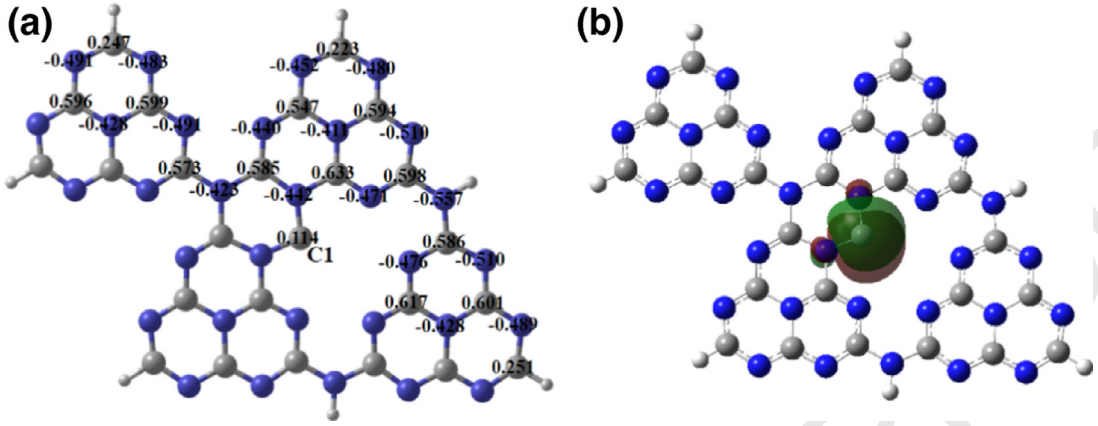

Fig. 2. (a) Optimized structure with natural population analysis (NPA) charges and (b) the highest-occupied molecular orbital (HOMO) of the cluster model for C/g-C_3N_4.

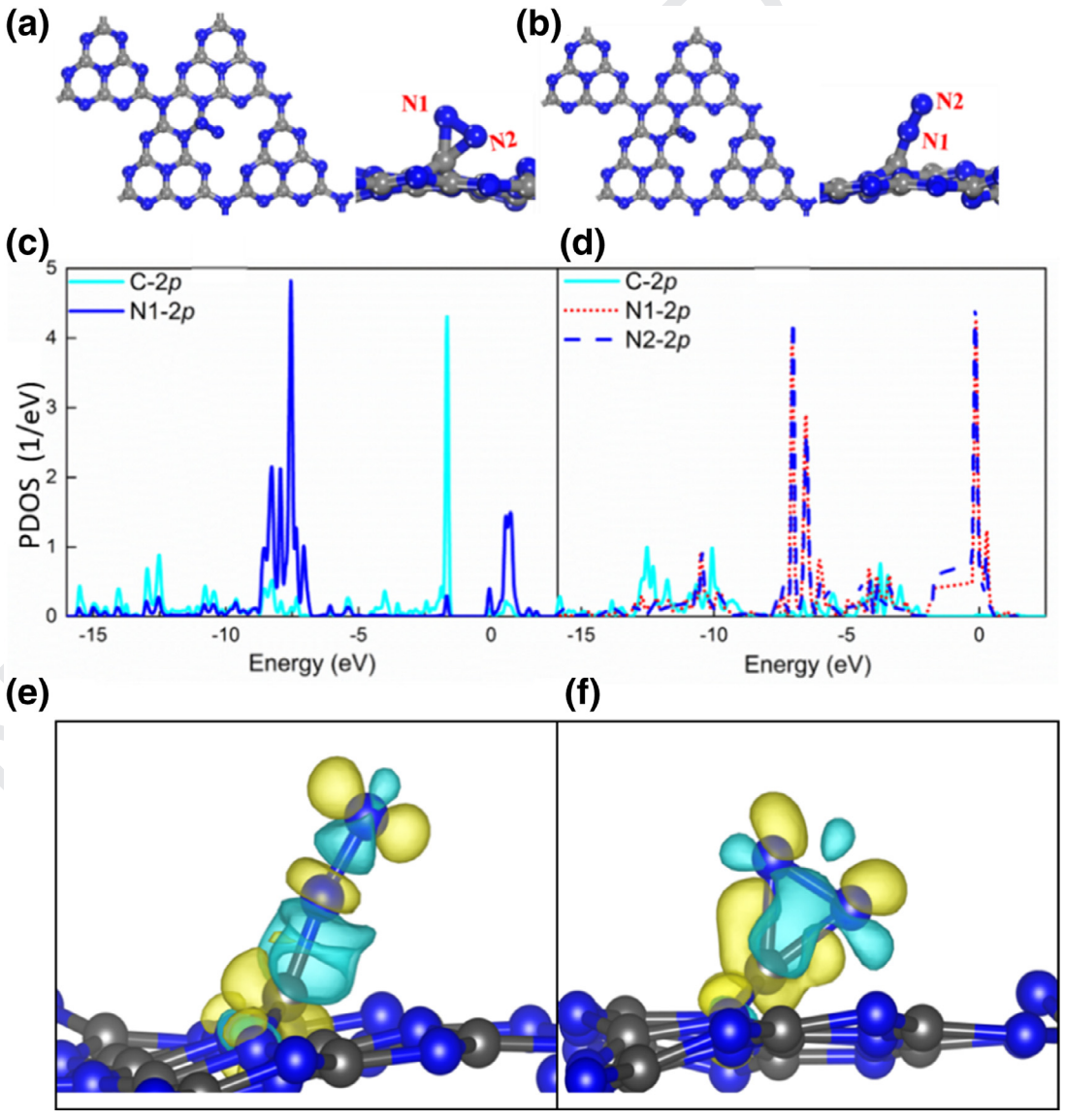

Fig. 3. (a) and (b) The optimized structures; (c) and (d) the projected density of states (PDOSs); (e) and (f) difference charge density of N_2 adsorption on C/g-C_3N_4 through end-on and side-on patterns, where the isosurface value is set to be 0.005 e Å^{-3} and cyan and yellow regions represent positive and negative charges, respectively. (For interpretation of the references to color in this figure legend, the reader is referred to the web version of this article.)

Please cite this article as: H. Li, L. Yang and Z. Wang et al., N-heterocyclic carbene as a promising metal-free electrocatalyst with high-efficiency for nitrogen reduction to ammonia, Journal of Energy Chemistry, https://doi.org/10.1016/j.jechem.2019.10.016

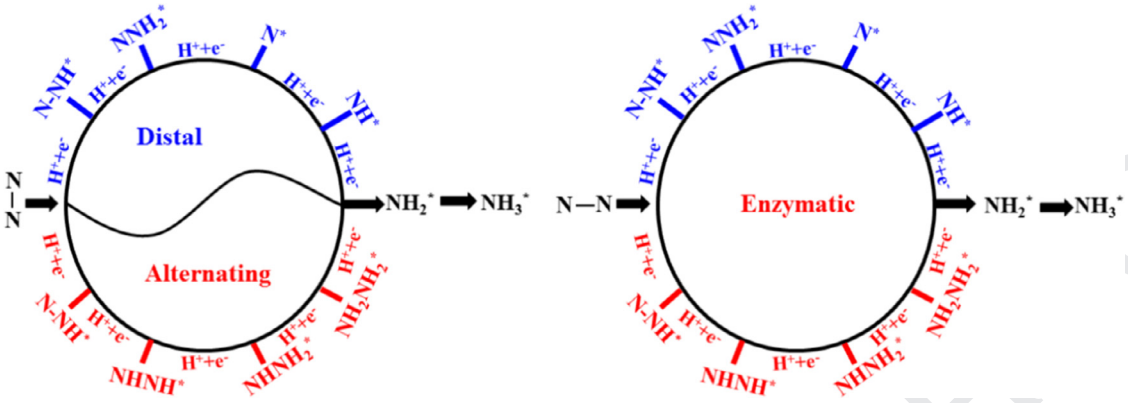

Fig. 4. The involved mechanisms of NRR on a catalyst surface, including distal, alternating, and enzymatic mechanisms.

To gain a deeper insight into the interaction between N_2 molecule and the NHCs-based catalyst, the projected density of states (PDOSs) for N_2 adsorbed C/g-C_3N_4 were examined (Fig. 3c and d), from which obvious hybridizations between the 2*p* orbitals of adsorbed N_2 molecule and the 2*p* orbitals of C-dopant can be observed for both end- and side-on adsorption configurations. Importantly, C/g-C_3N_4 always donates certain amount of electrons to the adsorbed N_2 molecule, thus accumulating negative charges (Fig. 3e and f) that help trigger the subsequent reduction reaction. Thus, the inherent σ-donor ability with a formal sp^2-hybridized long pair and unoccupied p-orbital at the carbene carbon can greatly activate the inert N≡N bond of N_2 molecule, and facilitates its subsequent reduction reactions.

3.3. N_2 reduction to NH_3

Since the inert N_2 molecule has been sufficiently activated on the surfaces of NHC-based C/g-C_3N_4, we continued to evaluate the possibility of its reduction to NH_3. Following previous studies, three reaction mechanisms are involved in the NRR, including distal, alternating, and enzymatic mechanisms. The first two pathways start from the end-on N_2 adsorption, while the last one will initiate the enzymatic pathway (Fig. 4), in which all possible reaction intermediates (N_2H^*, $N_2H_2^*$, $N_2H_3^*$, $N_2H_4^*$, N^*, NH^*, and NH_2^*) were included. To determine the most favorable reaction pathway, the free energy profiles along the three reaction pathways were explored, and the overpotential (η) was adopted as a measure for the whole NRR rate. Notably, the η value can be determined by: $\eta = U_{equilibrium} - U_{limiting}$, where $U_{equilibrium}$ is the equilibrium potential of NRR (about −0.16 V) and $U_{limiting}$ is the limiting potential that can be computed by: $U_{limiting} = -\Delta G_{max}/e$, where ΔG_{max} represents the maximum free energy change among all elementary steps in the NRR, i.e., the potential-determining step (PDS). Smaller η suggests low energy input and higher catalytic activity.

Thus, we evaluated the NRR catalytic activity of C/g-C_3N_4 by the free energy profiles based on the computed ΔG values of all elementary steps in the NRR. Because both end-on and side-on configurations are energetically favorable for N_2 adsorption on C/g-C_3N_4, all the three mechanisms (distal, alternating, and enzymatic) were considered. The obtained free energy diagrams for NRR on C/g-C_3N_4 along the three pathways were shown in Fig. 5, while the corresponding structures of reaction intermediates were presented in Fig. S6.

Starting from the end-on N_2 adsorption, the adsorbed N_2 molecule will be hydrogenated by adsorbing a proton coupled with an electron transfer to form a NNH group that is still adsorbed on the carbene C site with a C–N bond length of 1.24 Å. The hydrogen preferentially binds to the upper N site, and the N–N bond is further elongated to 1.27 Å. Remarkably, this step of $N_2^* + H^+ + e^- \rightarrow NNH^*$ is uphill in the free energy profile by 0.33 eV (Fig. 5a). Hereafter, the formed NNH^* species will be further hydrogenated by reacting with another proton. As the two N atoms in NNH species are possible adsorption sites for the second H atom, the NRR can proceed via two different pathways (Fig. 4), one is the distal mechanism, in which the electron pairs continually attack at the upper N of NNH^* species to produce the first NH_3 after two hydrogenation steps, followed by the hydrogenation of the other N atom to yield the second NH_3 by $3(H^+ + e^-)$. The other mechanism is the alternating reduction pathway, in which the two N atoms of N_2H^* species is hydrogenated alternatively, and the release of the second NH_3 molecule just follows the release of the first NH_3 one.

Once the N_2 reduction reaction proceed along the distal pathway, all elementary hydrogenation steps are exothermic, except for the generation of the second NH_3 with a ΔG value of 0.23 eV, which is slightly smaller than that of the formation of NNH^* species ($\Delta G = 0.33$ eV). Thus, in the distal pathway, the hydrogenation of N_2^* to NNH^* is the PDS for the NRR on C/g-C_3N_4 due to its maximum ΔG value, and the corresponding limiting potential is −0.33 V, while the overpotential is $[(-0.16) - (-0.33)] = 0.17$ V (Fig. 5a). In the alternating pathway, however, the PDS locates at the hydrogenation of $NH–NH_2^*$ species to $NH_2–NH_2^*$ with a ΔG value of 0.41 eV (Fig. 5b), corresponding to a slightly larger overpotential (0.25 V) than that of in the distal pathway (0.17 V). The release of the final product NH_3 from C/g-C_3N_4 surface needs to overcome a free energy barrier of 2.31 eV, which seems to be difficult. However, under acidic electrochemical conditions, the NH_3^* species is not directly desorbed to form free NH_3, instead, as experimentally observed [56–58], NH_3^* is hydrogenated into NH_4^+ by reacting with H^+. Moreover, the released energy (about 3.28 eV, Fig. 5) in the proceeding hydrogenation steps can completely overcome the needed energy to release the formed NH_3 (2.31 eV). Thus, the NH_3 desorption is not a problematic obstacle.

In the enzymatic reduction pathway initiated by the side-on N_2 adsorption, the electron pairs alternately attack the two N atoms adsorbed on the C site. According to the computed free energies of all elementary step in this pathway, we found that the hydrogenation of $NH–NH^*$ to $NH–NH_2^*$ can be identified as the PDS with the ΔG_{max} value of 0.21 eV, which is slightly lower than that of distal (0.33 eV) and alternating mechanism (0.41 eV), suggesting that the NRR catalyzed by C/g-C_3N_4 prefers to proceed via the enzymatic mechanism with. The computed overpotential is 0.05 V, which is comparable to those of other well-established NRR electrocatalysts [59–66]. Thus, the NHC-like g-C_3N_4 is expected to be a promising metal-free electrocatalyst with high-efficiency for the NRR. Very recently, Ling et al. indicated that a single boron atom embedded

Please cite this article as: H. Li, L. Yang and Z. Wang et al., N-heterocyclic carbene as a promising metal-free electrocatalyst with high-efficiency for nitrogen reduction to ammonia, Journal of Energy Chemistry, https://doi.org/10.1016/j.jechem.2019.10.016

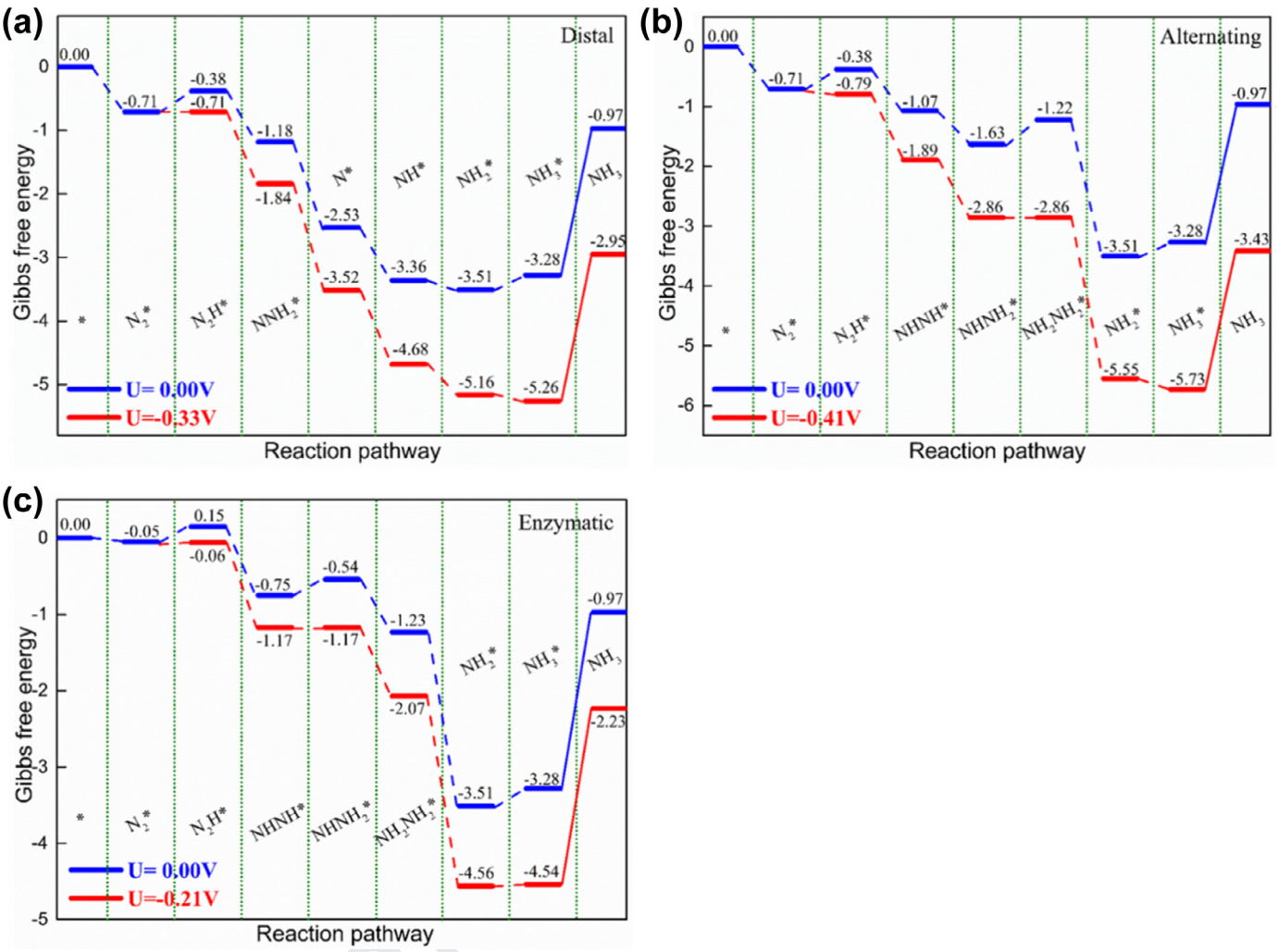

Fig. 5. The free energy profiles of NRR on C/g-C_3N_4 along the (a) distal, (b) alternating, and (c) enzymatic pathways.

in g-C_3N_4 monolayer exhibits the excellent catalytic properties for the NRR due to the "acceptance-donation" process, where one remaining empty orbital of B atom can accept the lone-pair electrons of N_2 molecule, while its occupied sp^3 orbitals of B atom will donate electrons to the π^* anti-bonding orbital of N_2 molecule [59]. As above discussion, the NHC atom embedded into g-C_3N_4 also contains sp^2-hybridized lone pair and p_z unoccupied orbital, which can also drive the "acceptance-donation" process to effectively convert N_2 to NH_3.

We also considered the hybrid catalytic pathway, i.e., the formed $N_2H_2^*$ species in the distal pathway would shuttle to an alternating pathway. Our computations suggested that, in this mixed mechanism, the transformation from the adsorbed N_2 with the end-on manner to the N_2H^* species is the potential-determining step, and its free energy change (0.33 eV) is larger than that in the enzymatic mechanism (0.21 eV). Thus, the hybrid pathway is less favorable energetically than the enzymatic one. Furthermore, to gain deeper insight into the reaction mechanism, LST/QST method was employed to search for the transition state (TS) along the enzymatic mechanism to evaluate the kinetic possibility of the NRR on our proposed catalyst. The energy barriers between every two neighboring intermediates were presented in Fig. 6. Our results showed that the formation of N_2H_2 and N_2H_3 intermediates can spontaneously proceed with a zero barrier energy. The maximum energy barrier among all elementary step locates at the release of the first NH_3 (0.64 eV), suggesting the high kinetic feasibility of the NRR on NHC-like g-C_3N_4 at ambient conditions.

In addition, the catalytic performance of the substituted doping of one of N atom in g-C_3N_4 by one C atom for the NRR was thus examined. As there are three nonequivalent N atoms in pristine g-C_3N_4, three possible substituted doping sites were considered, which were labeled as C_{N1}, C_{N2}, and C_{N3}, respectively, as shown in Fig. S7. Our results demonstrated that the three-coordinated C_{N1} and C_{N3} exhibit considerably weak adsorption strength for N_2 molecule with the adsorption energy less than −0.15 eV. Thus, the inert N_2 molecule cannot be effectively activated on the two C sites, thus ruling out them as ideal NRR electrocatalysts. In contrast, on the surface of C_{N2}, the N_2 molecule can be chemisorbed in the end-on manner on the two-coordinated C dopant due to its large magnetic moment (Fig. S8), and the corresponding adsorption energy is −1.44 eV. For the adsorbed N_2 molecule via end-on pattern, its subsequent reduction will take place via distal or alternative mechanism. According to the computed free energies, the formation of the first NH_3 molecule is the PDS in distal pathway with ΔG_{max} value of 0.54 eV, while the PDS locates at the hydrogenation of NH–NH_2^* to NH_2–NH_2^* in the alternating pathway with the ΔG_{max} of 0.61 eV (Fig. 7). Clearly, the C_{N2} sheet exhibits weaker catalytic activity for the NRR than NHC-based C/g-C_3N_4 due to its larger overpotential (0.38 V vs. 0.05 V).

Finally, we examined the hydrogen evolution reaction (HER) on C/g-C_3N_4, since it is the most important competing side reaction

Please cite this article as: H. Li, L. Yang and Z. Wang et al., N-heterocyclic carbene as a promising metal-free electrocatalyst with high-efficiency for nitrogen reduction to ammonia, Journal of Energy Chemistry, https://doi.org/10.1016/j.jechem.2019.10.016

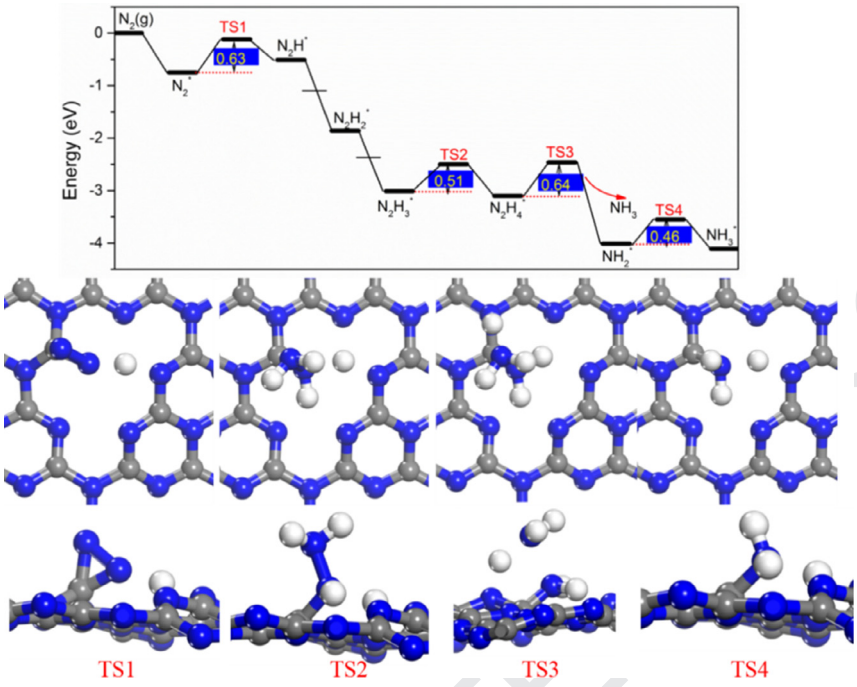

Fig. 6. The energy barriers along the minimum energy (i.e., enzymatic) path for NRR on C/C_3N_4, and the optimized structures for four transition states (top and side views).

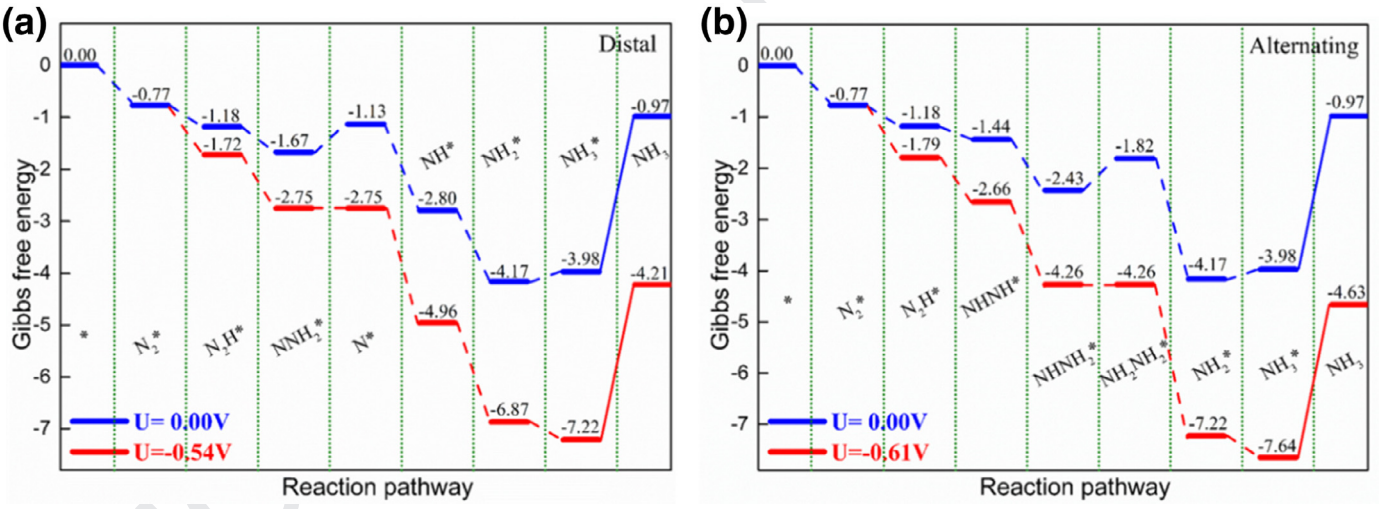

Fig. 7. The free energy profiles of NRR on C-doped g-C_3N_4 with C_{N2} configuration along the (a) distal and (b) alternating pathways.

of NRR and could lead to the low Faradic efficiency of ≤1% for the NRR. To evaluate the selectivity towards NRR, we compared the adsorption free energy of N_2H^* species on the catalyst surface with that of H^* due to the following reasons: (1) the N_2H^* species formation is the first and one of the most important hydrogenation steps in the NRR, and its stabilization on the catalyst surface usually determines the catalytic performance [47]; (2) in the electrochemical ammonia synthesis, the Heyrovsky-type mechanism is usually preferred rather than the slow Tafel-type mechanism with high activation barriers (> 1.00 eV) for $NH_x^* + H^* \rightarrow NH_{x+1}^*$ reaction [67]. Note that in the Heyrovsky-type mechanism, the adsorbed N_2H_x or NH_x species will be hydrogenated by direct attachment of protons from the solution and electrons from the electrode, and the applied bias has a direct influence on the energy barrier. Thus, if the adsorption of N_2H^* species is stronger than H^* species, the catalyst should be more selective towards NRR compared with HER [47].

Our computational results demonstrated that the ΔE_{N2H^*} (−2.84 eV) is much stronger than ΔE_{H^*} (−1.95 eV) on C/g-C_3N_4. We also considered the competition between N_2H^* and H_2O adsorption on the C/g-C_3N_4 surface, and found that N_2H^* binds much stronger to the surface ($\Delta E_{N2H^*} = -2.84$ eV) than H_2O ($\Delta E_{H2O} = -0.77$ eV) (Fig. S9). Thus, on the C/g-C_3N_4 surface, N_2H^* binds more strongly than both H and H_2O, which suggests that both HER and H_2O poisoning can be suppressed, and our predicted catalyst has a good NRR selectivity.

Note that it is also possible to further improve the NRR selectivity. As pointed out by Nørskov and coworkers [13], limiting either proton or electron availability at the catalyst surface can effectively attenuate HER or H_2O poisoning, and thus make NRR preferentially occur. Guided by this hypothesis, several promising strategies have been developed for suppressing HER and H_2O poisoning in recent experimental studies, such as adjusting electrolyte, adding protection layers or surface tethering of the heterogeneous catalysts, and

Please cite this article as: H. Li, L. Yang and Z. Wang et al., N-heterocyclic carbene as a promising metal-free electrocatalyst with high-efficiency for nitrogen reduction to ammonia, Journal of Energy Chemistry, https://doi.org/10.1016/j.jechem.2019.10.016

controlling the electron transfer rate [7,68–70]. Using non-aqueous electrolytes, such as titanocene dichloride ($(\eta 5\text{-}C_5H_5)_2TiCl_2$), Jeong et al. demonstrated that both the rate of ammonia synthesis and its faradaic efficiency can be greatly improved by suppressing the HER [68]; Using ionic liquids with trace amounts of water (as the proton source) as electrolytes to limit the proton transfer rate, thus suppress HER, MacFarlane and coworkers achieved high conversion efficiency of 60% for NRR to ammonia at ambient conditions on a Fe-based catalysts [69]; By coating a super-hydrophobic metal-organic framework (MOF) layer over the NRR electrocatalyst, Lee et al. achieved superior NRR selectivity (~90%) and a boost to Faradic efficiency by 10 percentage points at ambient operations [70]. Inspired by these encouraging findings, we suggest that experimentally similar strategies can be used to attenuate HER or H_2O poisoning on C/g-C_3N_4. Note that various studies showed that NHCs can catalyze organic reactions in aqueous media [71–74]. Overall, the possible HER or H and H_2O poisoning for NRR on our proposed C/g-C_3N_4 is not a big concern.

4. Conclusion

By means of comprehensive density functional theory (DFT) computations, we have proposed a novel, metal-free, and NHC-based electrocatalyst for NRR that is composed by C-decorated g-C_3N_4. Our results showed that the C-dopant exhibits carbene nature due to its unique structure and electronic properties, which facilitates to activate the inert N_2 molecule and the subsequent reduction reaction to NH_3 via the enzymatic pathway with a rather low overpotential of 0.05 V. With high stability, good electrical conductivity, low overpotential, and significant suppressing of HER, we strongly believe that our newly predicted C/g-C_3N_4 will be realized by experimental peers as NHC-based catalysts for NRR in the very near future. We also hope that our studies could inspire more experimental and theoretical studies on exploring the potential of NHC-based nanomaterials as metal-free catalysts for other important chemical reactions.

Declaration of Competing Interest

The authors declare that they have no known competing financial interests or personal relationships that could have appeared to influence the work reported in this paper.

Acknowledgments

This work was financially supported in China by the National Natural Science Foundation of China (21103224 and 21878227), Natural Science Funds for Distinguished Young Scholar of Heilongjiang Province (No. JC2018004), Natural Science Foundation of Hebei Province of China (B2019202210), and in USA by NSF-CREST Center for Innovation, Research and Education in Environmental Nanotechnology (CIRE2N) (Grant Number HRD-1736093). The authors also acknowledge the computational resource supported by the Supercomputing Center in Harbin Normal University and Lvliang. A portion of this research used computational resources at the Center for Nanophase Materials Sciences, which is a DOE Office of Science User Facility.

Supplementary material

Supplementary material associated with this article can be found, in the online version, at doi:10.1016/j.jechem.2019.10.016.

References

[1] V. Rosca, M. Duca, M.T. de Groot, M.T.M. Koper, Chem. Rev. 109 (2009) 2209–2244.
[2] B.M. Hoffman, D. Lukoyanov, Z.-Y. Yang, D.R. Dean, L.C. Seefeldt, Chem. Rev. 114 (2014) 4041–4062.
[3] T. He, P. Pachfule, H. Wu, Q. Xu, P. Chen, Nat. Rev. Mater. 1 (2016) 16059.
[4] L. Ye, R. Nayak-Luke, R. Bañares-Alcántara, E. Tsang, Chem 3 (2017) 712–714.
[5] J.W. Erisman, M.A. Sutton, J. Galloway, Z. Klimont, W. Winiwarter, Nat. Geosci. 1 (2008) 636.
[6] C. Tang, S.-Z. Qiao, Chem. Soc. Rev. (2019), doi:10.1039/C9CS00280D.
[7] X. Cui, C. Tang, Q. Zhang, Adv. Energy Mater. 8 (2018) 1800369.
[8] R.R. Eady, Chem. Rev. 96 (1996) 3013–3030.
[9] X. Liu, Y. Jiao, Y. Zheng, M. Jaroniec, S.-Z. Qiao, J. Am. Chem. Soc. 141 (2019) 9664–9672.
[10] S.L. Foster, S.I.P. Bakovic, R.D. Duda, S. Maheshwari, R.D. Milton, S.D. Minteer, M.J. Janik, J.N. Renner, L.F. Greenlee, Nat. Catal. 1 (2018) 490–500 1.
[11] C. Guo, J. Ran, A. Vasileff, S.-Z. Qiao, Energy Environ. Sci. 11 (2018) 45–56.
[12] J.H. Montoya, C. Tsai, A. Vojvodic, J.K. Nørskov, ChemSusChem 8 (2015) 2180–2186.
[13] A.R. Singh, B.A. Rohr, J.A. Schwalbe, M. Cargnello, K. Chan, T.F. Jaramillo, I. Chorkendorff, J.K. Nørskov, ACS Catal. 7 (2017) 706–709.
[14] Z.W. Seh, J. Kibsgaard, C.F. Dickens, I. Chorkendorff, J.K. Nørskov, T.F. Jaramillo, Science 355 (2017) eaad4998.
[15] M.-M. Shi, D. Bao, S.-J. Li, B.-R. Wulan, J.-M. Yan, Q. Jiang, Adv. Energy Mater. 8 (2018) 1800124.
[16] J. Han, X. Ji, X. Ren, G. Cui, L. Li, F. Xie, H. Wang, B. Li, X. Sun, J. Mater. Chem. A 6 (2018) 12974–12977 6.
[17] Y. Yao, S. Zhu, H. Wang, H. Li, M. Shao, J. Am. Chem. Soc. 140 (2018) 1496–1501.
[18] X. Liu, L. Dai, Nat. Rev. Mater. 1 (2016) 16064.
[19] H. Jin, C. Guo, X. Liu, J. Liu, A. Vasileff, Y. Jiao, Y. Zheng, S.-Z. Qiao, Chem. Rev. 118 (2018) 6337–6408.
[20] Q. Wu, L. Yang, X. Wang, Z. Hu, Acc. Chem. Res. 50 (2017) 435–444.
[21] S. Navalon, A. Dhakshinamoorthy, M. Alvaro, M. Antonietti, H. García, Chem. Soc. Rev. 46 (2017) 4501–4529 46.
[22] C. Hu, Y. Xiao, Y. Zou, L. Dai, Electrochem. Energy Rev. 1 (2018) 84–112.
[23] N. Daems, X. Sheng, I.F.J. Vankelecom, P.P. Pescarmona, J. Mater. Chem. A 2 (2014) 4085–4110.
[24] H. Jiang, J. Gu, X. Zheng, M. Liu, X. Qiu, L. Wang, W. Li, Z. Chen, X. Ji, J. Li, Energy Environ. Sci. 12 (2019) 322–333.
[25] Y. Song, W. Chen, C. Zhao, S. Li, W. Wei, Y. Sun, Angew. Chem. Int. Ed. 56 (2017) 10840–10844.
[26] S. Zhou, N. Liu, Z. Wang, J.J. Z.hao, ACS Appl. Mater. Interfaces 9 (2017) 22578–22587.
[27] S. Zhou, X. Yang, W. Pei, N. Liu, Z. Wang, J.J. Zhao, Nanoscale 10 (2018) 10876–10883.
[28] W. Pei, S. Zhou, Y. Bai, J.J. Zhao, Carbon 133 (2018) 260–266.
[29] M.N. Hopkinson, C. Richter, M. Schedler, F. Glorius, Nature 510 (2014) 485.
[30] M. Nicolas, D.-G. Silvia, P.N. Steven, Angew. Chem. Int. Ed. 17 (2007) 2988–3000.
[31] W.-P. Sabrina, U. Radius, T.B. Marder, Dalton Trans. 45 (2016) 5880–5895.
[32] D. Enders, O. Niemeier, A. Henseler, Chem. Rev. 107 (2007) 5606–5655.
[33] C.M. Crudden, D.P. Allen, Coord. Chem. Rev. 248 (2004) 2247–2273.
[34] W.J. Sommer, M. Weck, Coord. Chem. Rev. 251 (2007) 860–873.
[35] R. Zhong, A.C. Lindhorst, F.J. Groche, F.E. Kühn, Chem. Rev. 117 (2017) 1970–2058.
[36] Z. Zhao, Y. Sun, F. Dong, Nanoscale 7 (2015) 15–37.
[37] G. Gao, Y. Jiao, E.R. Waclawik, A. Du, J. Am. Chem. Soc. 138 (2016) 6292–6297.
[38] Z. Chen, J. Zhao, C.R. Cabrera, Z. Chen, Small Methods 3 (2018) 1800368.
[39] B. Delley, J. Chem. Phys. 113 (2000) 7756–7764.
[40] B. Delley, J. Chem. Phys. 92 (1990) 508–517.
[41] J.P. Perdew, K. Burke, M. Ernzerhof, Phys. Rev. Lett. 77 (1996) 3865–3868.
[42] S. Grimme, J. Comput. Chem. 27 (2006) 1787–1799.
[43] F.L. Hirshfeld, Theore. Chim. Acta 44 (1977) 129–138.
[44] J.K. Nørskov, J. Rossmeisl, A. Logadottir, L. Lindqvist, J.R. Kitchin, T. Bligaard, H. Jónsson, J. Phys. Chem. B 108 (2004) 17886–17892.
[45] A.A. Peterson, F. Abild-Pedersen, F. Studt, J. Rossmeisl, J.K. Nørskov, Energy Environ. Sci. 3 (2010) 1311–1315.
[46] V. Tripković, E. Skúlason, S. Siahrostami, J.K. Nørskov, J. Rossmeisl, Electrochim. Acta 55 (2010) 7975–7981.
[47] Y. Abghoui, S.B. Sigtryggsson, E. Skúlason, ChumSusChem (2019), doi:10.1002/cssc.201901429.
[48] E. Skúlason, T. Bligaard, S. Gudmundsdóttir, F. Studt, J. Rossmeisl, F. Abild-Pedersen, T. Vegge, H. Jónsson, J.K. Nørskov, Phys. Chem. Chem. Phys. 14 (2012) 1235–1245.
[49] N. Govind, M. Petersen, G. Gitzgerald, D. King-Smith, J. Andzelm, J. Comput. Mater. Sci. 28 (2003) 250–258.
[50] D. Masih, Y. Ma, S. Rohani, Appl. Catal. B Environ. 206 (2017) 556–588.
[51] Y. Wang, X. Liu, J. Liu, B. Han, X. Hu, F. Yang, Z. Xu, Y. Li, S. Jia, Z. Li, Y. Zhao, Angew. Chem. Int. Ed. 57 (2018) 1–8.
[52] H. Gao, R. Cao, S. Zhang, H. Yang, X. Xu, ACS Appl. Mater. Interfaces 11 (2019) 2050–2059.
[53] N. Bao, Hu X, Q. Zhang, X. Miao, X. Jie, S. Zhou, Appl. Surf. Sci. 403 (2017) 682–690.

[54] B. Zhu, J. Zhang, C. Jiang, B. Cheng, J. Yu, Appl. Catal. B Environ. 207 (2017) 27–34.
[55] Gaussian 03, Revision C.02, M.J. Frisch, G.W. Trucks, H.B. Schlegel, G.E. Scuseria, M.A. Robb, J.R. Cheeseman, J.A. Montgomery, T. Vreven, K.N. Kudin, J.C. Burant, J.M. Millam, S.S. Iyengar, J. Tomasi, V. Barone, B. Mennucci, M. Cossi, G. Scalmani, N. Rega, G.A. Petersson, H. Nakatsuji, M. Hada, M. Ehara, K. Toyota, R. Fukuda, J. Hasegawa, M. Ishida, T. Nakajima, Y. Honda, O. Kitao, H. Nakai, M. Klene, X. Li, J.E. Knox, H.P. Hratchian, J.B. Cross, C. Adamo, J. Jaramillo, R. Gomperts, R.E. Stratmann, O. Yazyev, A.J. Austin, R. Cammi, C. Pomelli, J.W. Ochterski, P.Y. Ayala, K. Morokuma, G.A. Voth, P. Salvador, J.J. Dannenberg, V.G. Zakrzewski, S. Dapprich, A.D. Daniels, M.C. Strain, O. Farkas, D.K. Malick, A.D. Rabuck, K. Raghavachari, J.B. Foresman, J.V. Ortiz, Q. Cui, A.G. Baboul, S. Clifford, J. Cioslowski, B.B. Stefanov, G. Liu, A. Liashenko, P. Piskorz, I. Komaromi, R.L. Martin, D.J. Fox, T. Keith, M.A. Al-Laham, C.Y. Peng, A. Nanayakkara, M. Challacombe, P.M.W. Gill, B. Johnson, W. Chen, M.W. Wong, C. Gonzalez, J.A. Pople, Gaussian, Inc., Wallingford CT. (2004).
[56] C. Choi, S. Back, N.-Y. Kim, J. Lim, Y.-H. Kim, Y. Jung, ACS Catal. 8 (2018) 7517–7525.
[57] I. Katsounaros, M.C. Figueiredo, X. Chen, F. Calle-Vallejo, M.T.M. Koper, ACS Catal. 7 (2017) 4660–4667.
[58] H.-J. Chun, V. Apaja, A. Clayborne, K. Honkala, J. Greeley, ACS Catal. 7 (2017) 3869–3882.
[59] C. Ling, X. Niu, Q. Li, A. Du, J. Wang, J. Am. Chem. Soc. 140 (2018) 14161–14168.
[60] Z. Chen, J. Zhao, L. Yin, Z.F. Chen, J. Mater. Chem. A 7 (2019) 13284–13292.
[61] X.-F. Li, Q.-K. Li, J. Cheng, L. Liu, Q. Yan, Y. Wu, X.-H. Zhang, Z.-Y. Wang, Q. Qiu, Y. Luo, J. Am. Chem. Soc. 138 (2016) 8706–8709.
[62] J. Zhao, Z. Chen, J. Am. Chem. Soc. 139 (2017) 12480–12487.
[63] J. Zhao, J. Zhao, Q. Cai, Phys. Chem. Chem. Phys. 20 (2018) 9248–9255.
[64] Z. Wang, Z. Yu, J. Zhao, Phys. Chem. Chem. Phys. 20 (2018) 12835–12844.
[65] W. Zhao, L. Zhang, Q. Luo, Z. Hu, W. Zhang, S. Smith, J. Yang, ACS Catal. 9 (2019) 3419–3425.
[66] C. Liu, Q. Li, J. Zhang, Y. Jin, D.R. MacFarlane, C. Sun, J. Mater. Chem. A. 7 (2019) 4771–4776.
[67] K. Honkala, A. Hellman, I.N. Remediakis, A. Logadottir, A. Carlsson, S. Dahl, C.H. Christensen, J.K. Nørskov, Science 307 (2005) 555.
[68] E.Y. Jeong, C.Y. Yoo, C.H. Jung, J.H. Park, Y.C. Park, J.N. Kim, S.G. Oh, Y. Woo, H.C. Yoon, ACS Sustain. Chem. Eng. 5 (2017) 9662–9666.
[69] F. Zhou, L.M. Azofra, M. Ali, M. Kar, A.N. Simonov, C. McDonnell-Worth, C. Sun, X. Zhang, D.-R. MacFarlane, Energy Environ. Sci. 10 (2017) 2516–2520.
[70] H.K. Lee, C.S.L. Koh, Y.H. Lee, C. Liu, I.Y. Phang, X. Han, C.-K. Tsung, X.Y. Ling, Sci. Adv. 4 (2018) eaar3208.
[71] E. Levin, E. Ivry, C.E. Diesendruck, N.G. Lemcoff, Chem. Rev. 115 (2015) 4607–4692.
[72] X. Bi, L. Wu, C. Yan, X. Jing, H. Zhu, J. Chil. Chem. Soc. 56 (2011) 663–664.
[73] K. Lee, A.R. Zhugralin, A.H. Hoveyda, J. Am. Chem. Soc. 131 (2009) 7253–7255.
[74] J.M. O'Brien, A.H. Hoveyda, J. Am. Chem. Soc. 133 (2011) 7712–7715.

Please cite this article as: H. Li, L. Yang and Z. Wang et al., N-heterocyclic carbene as a promising metal-free electrocatalyst with high-efficiency for nitrogen reduction to ammonia, Journal of Energy Chemistry, https://doi.org/10.1016/j.jechem.2019.10.016